Results in Surfaces and Interfaces 18 (2025) 100423

Contents lists available at ScienceDirect

Results in Surfaces and Interfaces

journal homepage: www.elsevier.com/locate/rsurfi

Modulated nanopillars via anodization of aluminum alloy and a possible application as antibacterial surfaces

Gabriel Jiménez-Thuel [a], Josué Cordero-Guerrero [a], Sergio Solano-Calderón [a], Sergio A. Paniagua [b,c,*]

[a] Chemistry Graduate Program, Universidad de Costa Rica, Montes de Oca, San José, Costa Rica
[b] Natural Sciences Department, Universidad de Costa Rica, Sede Occidente, Alajuela, Costa Rica
[c] National Nanotechnology Laboratory (LANOTEC), Centro Nacional de Alta Tecnología (CENAT), San José, Costa Rica

ARTICLE INFO

Keywords:
Anodization
Aluminum
Nanostructures
Antibacterial

ABSTRACT

Natural nanostructures on the skin and wings of selected fauna have been reported to confer mechano-bactericidal activity without the use of chemical antibiotics. It would be desirable to manufacture similar structures on man-made surfaces for medical and domestic use. In this paper, we show that aluminum anodization and wet etching can generate scalable, low-cost, and periodic nanostructures with high tunability. We present a comprehensive study of four types of nanopillars that produce bacteriostatic action in 1 h contact time against *Escherichia coli*, likely due to mechanical stress. Nanopillars with different dimensions were generated by modulation of temperature and voltage during the anodization of aluminum alloy AA6063. The surfaces with different aluminum oxide nanostructures decreased *E. coli* viability by ~47% on average vs smooth aluminum controls, demonstrating a robust and scalable approach to antibacterial nanostructured surfaces.

1. Introduction

Keeping surfaces bacteria-free to avoid the spread of disease is of interest in high-touch areas (*e.g.* handrails) and biomedical devices (including wheelchair frames, walkers, *etc.*) (Hasan et al., 2020). Traditional approaches for surface decontamination are usually active treatments, some of which are expensive or toxic, such as chemical (*e.g.* antibacterial agents), physical (*e.g.* UV/ozone), or thermal (*e.g.* steam) protocols(Skara, 2016). Since the initial discovery of mechano-bactericidal action due to nanopillars present in cicada wings (which appeared to impale bacteria)(Ivanova et al., 2012) several examples have been reported in nature, with a similar effect on both gram-negative and gram-positive bacteria (Kelleher et al., 2016; Lin et al., 2018; Green et al., 2017; Bandara et al., 2017; Pogodin et al., 2013; Tripathy et al., 2017). Gecko skin(Green et al., 2017) and dragonfly wings (Bandara et al., 2017) also possess nanoscale spikes or pillars that have bactericidal action via mechanical stress on the cell membrane of bacteria. Mathematical modeling of the mechanics shows that cell rigidity, dimensions and surface energy of the cell wall, nanostructure distribution, and the surface nanostructure shape are key factors in determining bacterial resistance/sensitivity to the bactericidal surface (Bandara et al., 2017; Pogodin et al., 2013; Elbourne et al., 2017; Watson et al., 2019; Linklater et al., 2021; Xue et al., 2015; Amir et al., 2014; Cui et al., 2021; Velic et al., 2021). These mechanisms could be less susceptible to bacterial resistance than traditional antibiotics (Ivanova et al., 2012; Linklater et al., 2021). The killing efficiency for dragonfly wings, for instance, has been determined to be *ca.* 60% vs. control over 3 h (on the order of 10^5 cells cm^{-2} min^{-1}) (Green et al., 2017).

Bioinspired, artificially-made nanotopographic surfaces have been investigated as a low-cost, scalable method to reduce bacterial viability and mitigate the propagation of pathogens on fomites (Hizal et al., 2017; Reed et al., 2019). There are commercial products with microstructured surfaces based on the micropatterns found on shark skin (Sharklet Technologies). While such surfaces reduce the transfer of microorganisms, they do not go as far as inactivating the pathogens. Since the publication of the first case of mechanobactericidal activity of nanostructures (Ivanova et al., 2012), the number of new techniques and materials developed to study the phenomena has increased significantly (Lin et al., 2018; Reed et al., 2019; Linklater et al., 2018; Ivanova et al.,

* Corresponding author. National Nanotechnology Laboratory (LANOTEC), Centro Nacional de Alta Tecnología (CENAT), San José, Costa Rica.
E-mail addresses: gabriel.jimenezthuel@ucr.ac.cr (G. Jiménez-Thuel), josue.corderoguerrero@ucr.ac.cr (J. Cordero-Guerrero), sergio.solanocalderon@ucr.ac.cr (S. Solano-Calderón), spaniagua@cenat.ac.cr (S.A. Paniagua).

https://doi.org/10.1016/j.rsurfi.2025.100423
Received 25 August 2024; Received in revised form 7 January 2025; Accepted 9 January 2025
Available online 13 January 2025

2013a; Cui et al., 2020; Fisher et al., 2016; Zhao et al., 2021). Reports range from silica and black silicon nanospikes prepared via reactive ion etch from Si wafers(Pogodin et al., 2013; Ivanova et al., 2013a) to chemical vapor deposited diamond nanocones (Fisher et al., 2016). These artificial nanostructured materials exhibit two unique antibacterial mechanisms: dense and blunt pillars that stretch and tear bacteria or sparse and sharp pillars that directly impale them (Michalska et al., 2018, 2021). Currently, most of the nanostructured surfaces use expensive materials and difficult-to-scale solutions such as reactive ion etching, hydrothermal etching, and laser treatments (Tripathy et al., 2017; Ivanova et al., 2013a; Lutey et al., 2018; Wandiyanto et al., 2020). Industrially relevant approaches with scalable methodology and nanotextured metals are not abundant. The manifold of naturally occurring and man-made antimicrobial surfaces was recently reviewed by Linklater et al. (2021) (Linklater et al., 2021).

Aluminum alloy surfaces are used in both household and hospital settings in a variety of applications, including kitchen appliances, handheld appliances, handrails, and biomedical devices. These surfaces usually undergo electrochemical reactions to make them less prone to oxidation. Even though it is known that changes in the anodic medium, voltage, and temperature can generate aluminum oxide nanostructures (Yi et al., 2012; Su et al., 2008; Rauf et al., 2009; Kwon et al., 2009; Sulka, 2008; Teshima et al., 2014; Hillebrand et al., 2008; Jeong and Choi, 2012), few reports study their effect as mechano-bactericidal surfaces (Linklater et al., 2021). Nanostructures randomly aligned as ridges created by wet etching of Al 6063 were reported to show between 80% and 90% of antibacterial activity in 4 h of incubation (91.9% of non-viable cells for *P. aeruginosa* and 87% for *S. aureus* according to fluorescence microscopy) (Hasan et al., 2020). Hot water treatments generated bactericidal pure Al-based grass/blade/scale-like nanostructures with similar dimensions (diameter and height of 100 nm and 200 nm, respectively) that killed between 59% and 67% of *E. coli* in 30 min according to fluorescence microscopy. Considering Al control also had 12% of non-viable cells, the antibacterial activity was approximately 47%–55% (Reed et al., 2019). Agbe et al. recently showed significant bactericidal efficiency with AAO nanowells (not nanopillars) after 4 h of contact time (Agbe et al., 2022a), and Murata et al., also reported significant antibacterial activity (after 24 h contact) against *E. coli* and *S. aureus* using anodic porous alumina (from pure aluminum) with different interpore distances generated through multiple repetitions of anodization and etch which result in densely spaced tapered pores (Murata et al., 2024).

This work aims to present protocols to prepare four different aluminum oxide nanopillars with tailored dimensions generated by scalable anodization and wet etching procedures, characterized via scanning electron microscopy (SEM). These nanostructures display an antibacterial effect (per modified Japanese Industrial Standard) against gram-negative bacteria such as *E. coli* and serve as proof of concept for developing scalable and potentially low-cost partial passivation against bacteria. Similar nanostructures have been reported (Zhao et al., 2021; Vassallo et al., 2017), but often prepared on atomically flat surfaces (such as silicon) or using cost-prohibitive or difficult-to-scale processes that would make them unlikely to be implemented as passive anti-pathogen surfaces on large areas, while the novelty of this study is that it is accomplished using a commercially available, common aluminum alloy. We first present the resulting structures and antibacterial properties, followed by a discussion section with further comments and explanations related to the findings of the study.

2. Experimental

Materials employed. Aluminum alloy AA6063 was sourced from Extralum (Cartago, Costa Rica). Perchloric acid (ACS reagent 60%), absolute ethanol (200 Proof), oxalic acid (anhydrous (≥ 99.0%), and phosphoric acid (≥ 85 wt %) were purchased from Sigma-Aldrich (Missouri, USA) and used as received. Chromium (VI) oxide (min 98%) was sourced from Matheson, Coleman & Bell Company (Cincinnati, USA) and vacuum filtered-dried before use. Water used as solvent in all cases was purified via reverse osmosis in a Merck Millipore RiOs system (Darmstadt, Germany).

Sample preparation. 3 cm × 6 cm commercial aluminum alloy (AA6063) plates were degreased via 5 min sonication in acetone The generation of nanostructures consisted of a 4-step procedure, with an electropolishing pretreatment using a StarPower MP20020D DC Power Supply (Maseen, China). The substrate and the counter-electrode were held 1.5 cm apart (Fig. 1). A propeller was used for stirring in all cases at 400 rpm. Anodization temperatures were controlled in a recirculating ethylene glycol/water bath. Each plate was electropolished in a perchloric acid medium (7% in absolute ethanol) at 0 °C, 20 V for 180 s. The first anodization consisted of an anodization with 0.3 M oxalic acid (see different conditions in Table 1), followed by a 30 min etch with 1.8% w/V chromic acid in a 6% V/V phosphoric acid solution at 60 °C (±2 °C) in all cases. The second anodization was performed with 0.3 M phosphoric acid (see different conditions in Table 1), and the final etch in all cases was done with 5% V/V phosphoric acid at 30 °C (±1 °C) for 40 min. The resulting nanopillar structures are shown in Fig. 2. Multiple batches of each sample type were prepared and characterized to ensure reproducibility.

Scanning electron microscopy (SEM). Samples were mounted on carbon tape and sputtered with gold using a Denton Vacuum Desk V sputter system at 20 mA for 180 s. Images were taken using a JSM-6390LV (JEOL, Tokyo, Japan) SEM, with an accelerating voltage of 30 kV, under a high vacuum, at a 45° tilt angle (the nanopillar heights were corrected for 45° view angle).

Antibacterial efficiency tests. These were done following the Japanese Industrial Standard (JIS Z 2801:2000) (Japanese Standards Association, 2000) with a few modifications. Bacteria and autoclaved glassware were handled in a Level 1 biosafety hood. *Escherichia coli* ATCC 25922 was incubated for at least 3 h in Lysogeny Broth at 37 °C with shaking at 120 rpm. The media was then replaced with water using 3 cycles of centrifugation at 4000 rpm followed by decantation, water refill, and vortex redispersion for inoculum to be added to the surfaces. Optical density was measured at 600 nm versus water as blank in a Shimadzu UV 1800 spectrophotometer and diluted 50 times from OD 0.05 ($\approx 2.5 \times 10^7$ cell/mL), resulting in approximately 5×10^5 cell/mL. Controls were run to ensure bacteria did not suffer significant shock from the cycles of centrifugation and vortex. 10 μL of this inoculum was placed on each surface. Two batches per sample type were done. For each run, 4 replicas of topographic samples and 4 smooth (electropolished-only) aluminum controls were typically used, and direct micropipetting of the inoculum was done as well on an agar plate as another control. After a contact time of 60 min in the biosafety hood, the samples and controls were immersed in a minimum of 2 mL of Lysogenia Broth and shaken to retrieve the inoculum from the surfaces. Several dilutions of this extract were made to find the proper dilution for acceptable colony-forming units in the next step, which consisted of placing 100 μL of the extract in a Petri dish and pouring agar at 44–47 °C followed by shaking to ensure proper dispersion. These were Parafilm®-sealed and incubated overnight at 37 °C in an agar-filled Petri dish resulting in 25–250 colony-forming units. Equation (1), accounting for dilution factors, was employed to determine the antibacterial activity:

$$\text{Antibacterial activity} = \frac{CFU\ Controls - CFU\ Samples}{CFU\ Controls} * 100 \quad (1)$$

For SEM characterization, aliquots of OD 0.05 at 600 nm were deposited on the substrate of interest and left to dry before coating with gold as mentioned above.

Fluorescence microscopy. A cell viability kit (DeNovix AO/PI Cell Drop Assay, Delaware, USA) was used as instructed to differentiate the viability of *E. coli* through fluorescent dyes: bacteria with compromised cell membrane allows propidium iodide dye to bind to its DNA and fluoresce red, while healthy membranes will not allow its binding, and

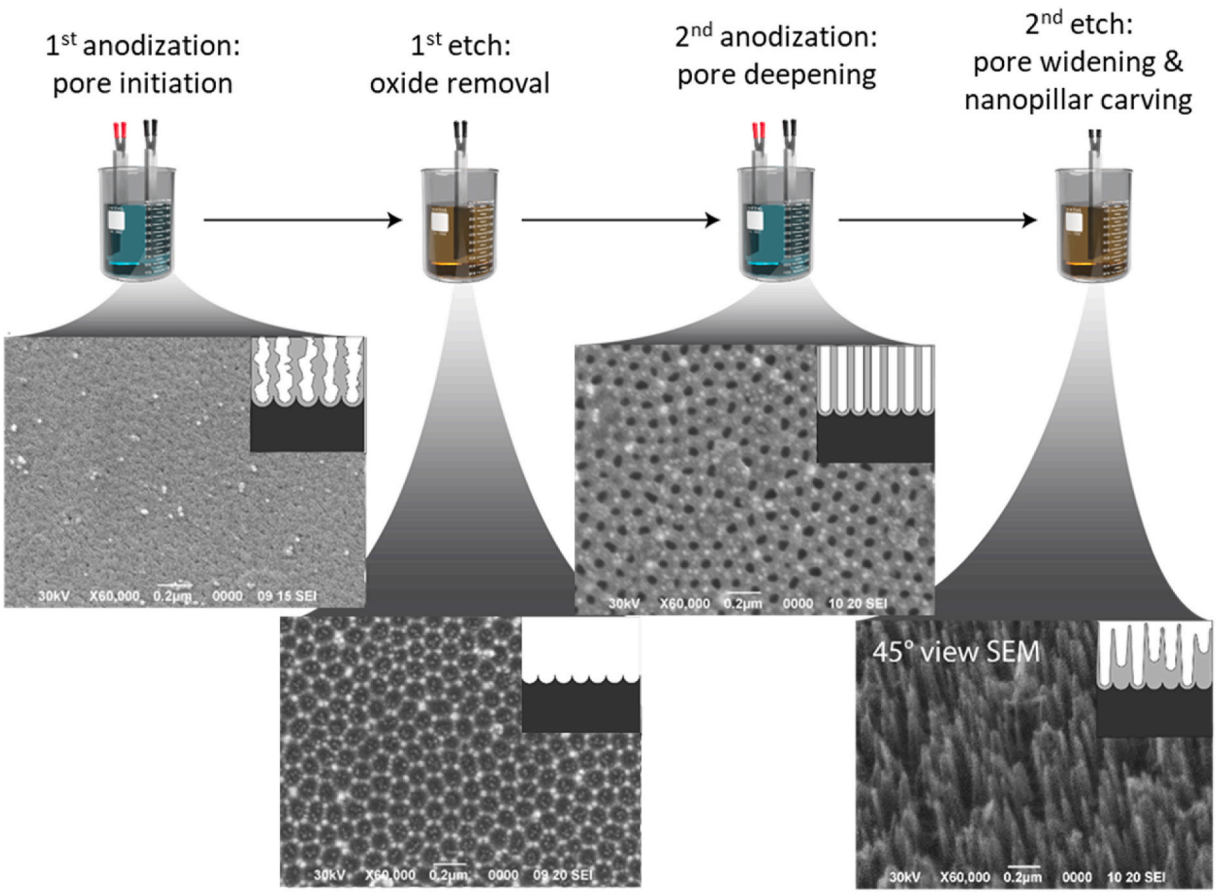

Fig. 1. Schematic of the anodization that aluminum alloy surfaces undergo to obtain nanopillars. In the first anodization, partially closed nanopores are generated, which are opened in the first etch step. These pores act as templates for a second anodization in which the nanopores generated are deepened and become more homogeneous (Masuda and Satoh, 1996). A final etch selectively removes sections of the pores, resulting in nanopillars.

Table 1
Voltage, time, and temperature conditions for anodization.

Sample ID	1A50	1A70	2A50	2A100
1st anodization conditions	50 V	70–75 V	50 V	50 V
	7 °C	0 °C	0 °C	0 °C
	120 min	120 min	120 min	120 min
2nd anodization conditions	50 V	50 V	50 V	100 V
	7 °C	7 °C	0 °C	0 °C
	60 min	60 min	60 min	60 min

the bacteria will fluoresce green due to acridine orange staining. The inoculum (OD_{600} = 0.10 for all samples) was stained with the kit per instructions, added to the samples, let stand for 60 min, and observed in a Zeiss Axio Scope A1 microscope with an HBO 100 mercury lamp and filter set for excitation at 450–490 nm and emission starting at 515 nm. Multiple images were acquired. No image merging was necessary.

Wear tests. A Discovery HR-3 rheometer from TA Instruments was employed to provide a measurable force with a programmed oscillation in parallel plates (25 mm) geometry. The samples undergoing testing were cut to areas of 0.4–0.8 cm^2 and mounted with double sided tape on the bottom plate, while at the top plate a Scotch-Brite® dishwashing sponge (soft side down) was affixed with a double-sided tape. The axial force was chosen so that stress pressure was 150 ± 15 kPa (a range of 50–250 kPa has been reported for the pressure a human hand applies while using tools (Hall, 1997; Hale et al., 2018)). 30 s and 300 s cycles consisting of 45° rotation at 1 Hz were performed on each sample, after which the samples were gold-sputtered and analyzed by SEM.

3. Results

3.1. Generation of nanopatterns

The four protocols presented in this work follow the procedure shown in Fig. 1. The electropolish pretreatment lowers their surface roughness from about 70 nm to roughly 1 nm on a 25 μm^2 area as observed by AFM, resulting in a much more homogeneous surface to begin with (as previously reported (Cordero-Guerrero et al., 2023)). The first steps in Fig. 1 consist of wells generation (step 1) and pore smoothing via etching (step 2), where the oxide begins to dissolve randomly, but the sites where initial etching occurred will have an increase in temperature due to the local current, which accelerates the dissolution in those sites, forming pores. The hexagonal arrangement occurs spontaneously due to the distribution of electric potential and current around these pores, as well as a steric effect (Sulka, 2008). The second anodization uses the opened pores in step 2 as templates to generate organized nanowells (Teshima et al., 2014) (as shown in Fig. 2 and discussed later). These are widened and carved in the last etch of the procedure, which determines the size and shape of the final nanostructures. Precise control of conditions during the last etch of the procedure is critical, as a slight change in any of the factors involved (temperature, concentration, or agitation) may result in under-etching (pillars not fully developed) or over-etching (nanopillar collapse). The different morphologies have varying process windows for time of the final etch, as shown in Fig. S1. Optimal time for pillar formation without collapse is approximately 40 min of etch in all cases using dilute phosphoric acid solution at 30 °C (structures shown in Fig. 2). 1A50 and 1A70 achieved the tallest pillars, but the window of etch time to produce

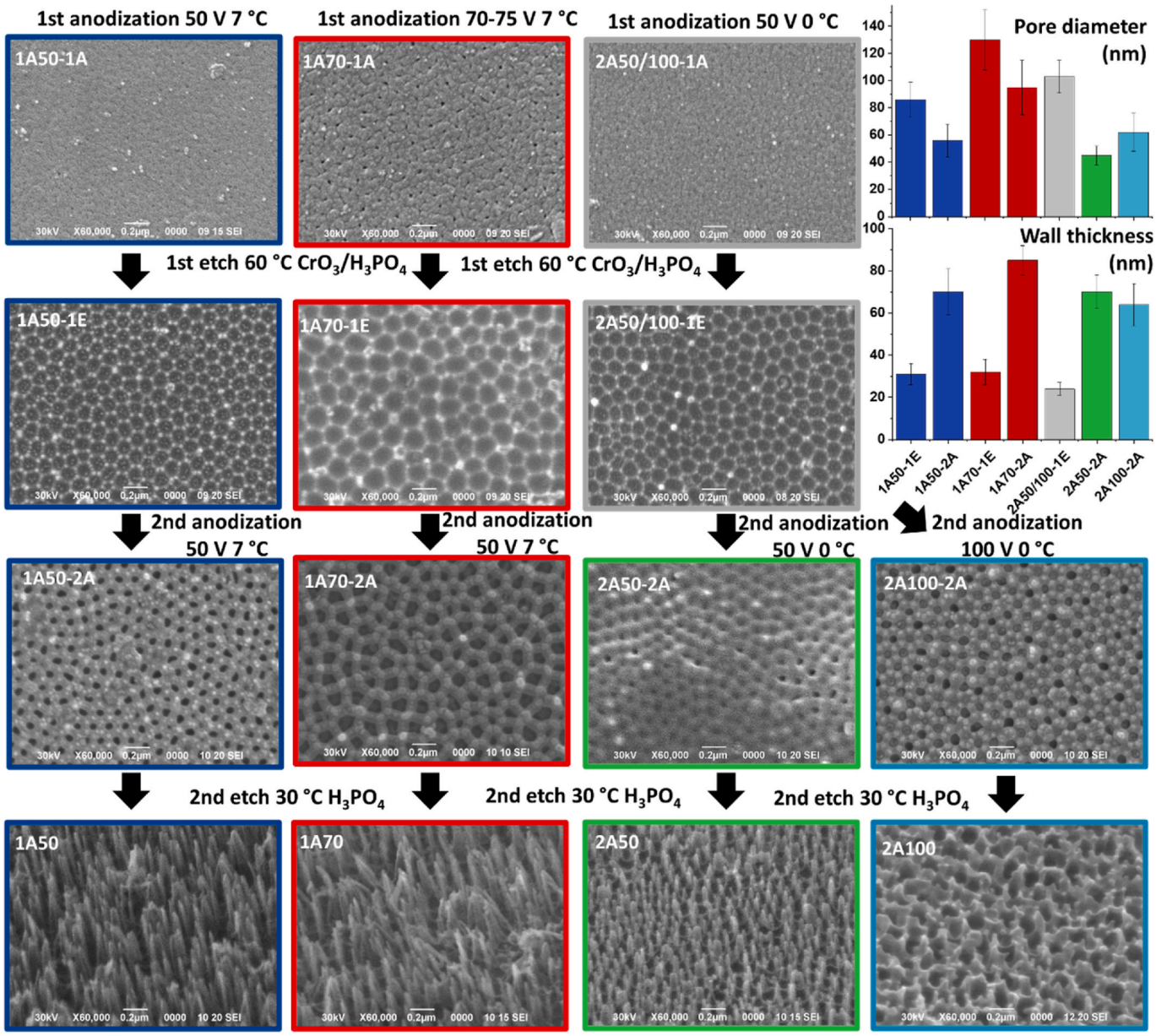

Fig. 2. Comparison of nanowells in sequential steps (-1A after first anodization, -1E after first etch, -2A after second anodization, all in top view SEM) for each protocol employed, and final nanopillars after second etch as observed by SEM at a 45° viewing angle). On the top right, color-coded bar graphs follow the wall-to-wall pore diameter and pore-to-pore wall thickness after first etch and second anodization.

tall, non-collapsed pillars is narrower than 2A50 and 2A100.

3.2. Characterization of nanopatterns

The procedures employed were tested multiple times, showing considerable reproducibility. Height, tip width, and full width at half maximum (FWHM) of the nanostructure were measured in addition to the pitch (distance between their tips) for each type of nanostructure. As Figs. 2 and 3 show, 1A50, 1A70, and 2A50 have a well-defined pillar structure, but their dimensions vary widely: 2A50 has the shortest nanostructures (161 ± 14) nm, while 1A70 nanopillars more than double that height (384 ± 25) nm. 2A100 differs morphologically from the rest: it has bigger spaces between the structures, and they also are wider at half their height (more cone-shaped).

3.3. Antibacterial activity

Antibacterial assays were done following a shortened JIS Z 2801 protocol (60 min contact time) with *E. coli* using the four types of nanostructures (at least two times each), and controls consisting of smooth electropolished aluminum also in contact with inoculum for 60 min, so that differences in activity can only be due to nanostructures since they are all hydrophilic and consist of aluminum oxide on the surface. The average antibacterial activity with the smooth reference ranged between 43 and 57% for the four types of surfaces (Fig. 4(a)). However, no meaningful differences in antibacterial effect were found between the different topographies (at 95% confidence level with an ANOVA statistical test) despite the varying dimensions. 1A50 and 1A70 surfaces displayed higher standard deviations, possibly due to less uniformity (collapsed nanostructures) where bacteria may have a higher probability of thriving. Fig. 4(b) considers the overall antibacterial activity of patterned surfaces vs controls of inoculum directly deposited on

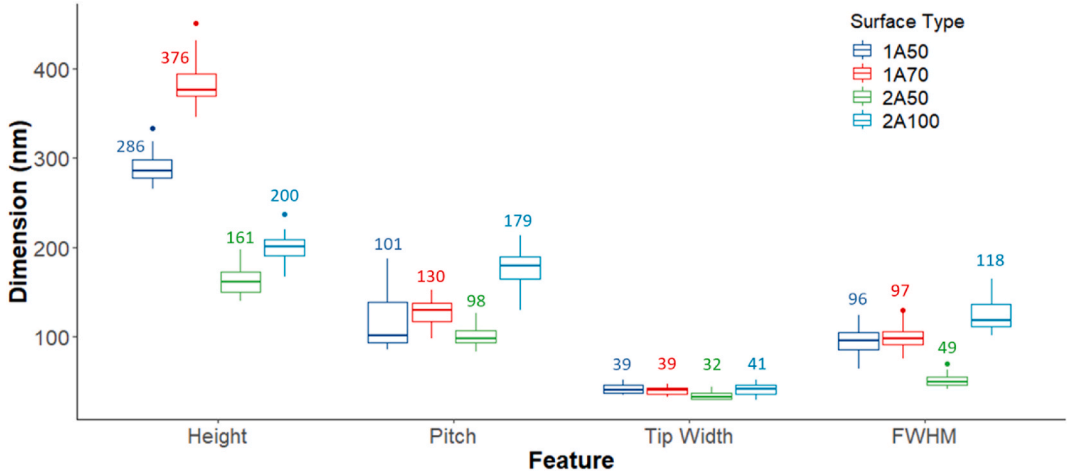

Fig. 3. Box plots for feature dimensions of the nanopillars obtained via voltage and temperature modulation during the anodization steps. 30 structures are considered for each sample type, from three different batches.

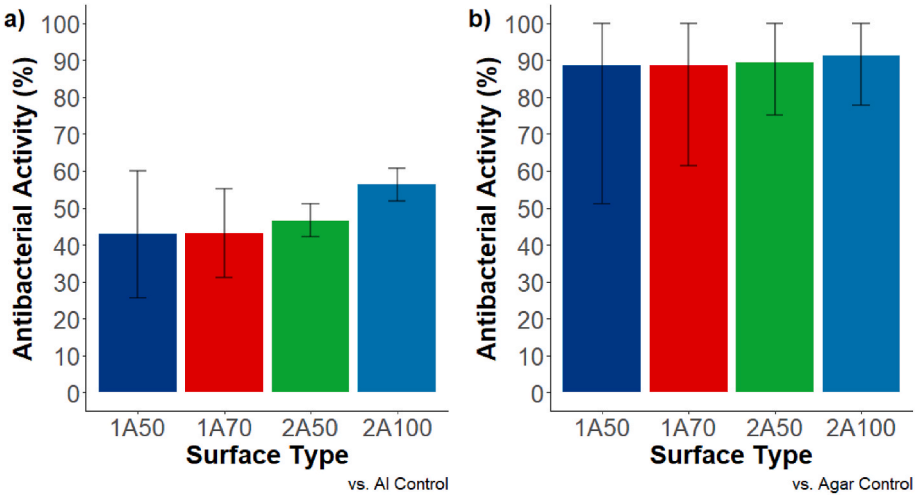

Fig. 4. Bar plots for antibacterial activity after 60 min contact time on different nanostructured samples (error bars are one standard deviation of the two batches ran, consisting of 4 replicas each): (a) *vs* smooth aluminum as control (b) *vs* agar plate as control (overall antibacterial activity).

Petri dishes (Agar control, no contact with Al surfaces). The difference may be due to the intrinsic chemical activity of the electropolished surface, with its fresh oxide functional groups which are passivated in as received aluminum.

3.4. Wear tests

To assess reusability of the nanopillar substrates, they were subjected to wear tests in which a dry sponge was oscillated up to 45° on top of the surface with a pressure of 150 ± 15 kPa. Both 30 s and 300 s cycles were attempted on separate samples. Only 2A100 was able to withstand such conditions, as shown in Fig. 5. The results for the other samples are shown in Supporting Information Fig. S4.

4. Discussion

4.1. Parameters that affect nanopattern dimensions

The temperatures and voltages in the protocols employed determine four different nanopatterns. The time used in a constant current anodization mainly affects the depth of the wells and the homogeneity of the structures, and it was kept constant in all cases. In conjunction with temperature, time affects kinetics and homogeneity, while electrolyte and concentration affect the achievable voltage at a given current (Su et al., 2008; Sulka, 2008). This study uses procedures that last no longer than 4.5 h. Different results can be obtained by increasing the anodization time, but a *quick* and scalable process was prioritized.

Several combinations of phosphoric-phosphoric, oxalic-oxalic, and oxalic-phosphoric acids for first and second anodization respectively, with conditions ranging from 50 to 150 V and 0–15 °C, were attempted based on previous reports (Teshima et al., 2014; Kotha et al., 2015). The appearance of nanopillars in the second etch was most consistently observed when oxalic acid was used in first anodization, followed by phosphoric acid in the second anodization. The use of oxalic acid in the first anodization generates an ordered porous alumina. Using 50 V vs 70 V in the first anodization will proportionally modulate the pore diameter, as described by Sulka (2008). We observe this difference when comparing 1A50-1A, 1A70-1A, and 2A50/100-1A which have only undergone the first anodization (Fig. 2). The pores only opened enough for SEM observation when 70 V were used (1A70-1). These pores are significantly widened in the first etch, and thus we have compared them in the plots included in Fig. 2, where for instance 1A70-1E, with first anodization at 70 V, has pores 50% larger than the 50 V counterpart after etch (1A50-1E).

To widen the pores, the less acidic phosphoric acid is employed in the second anodization; it is known that higher pH values increase the pore

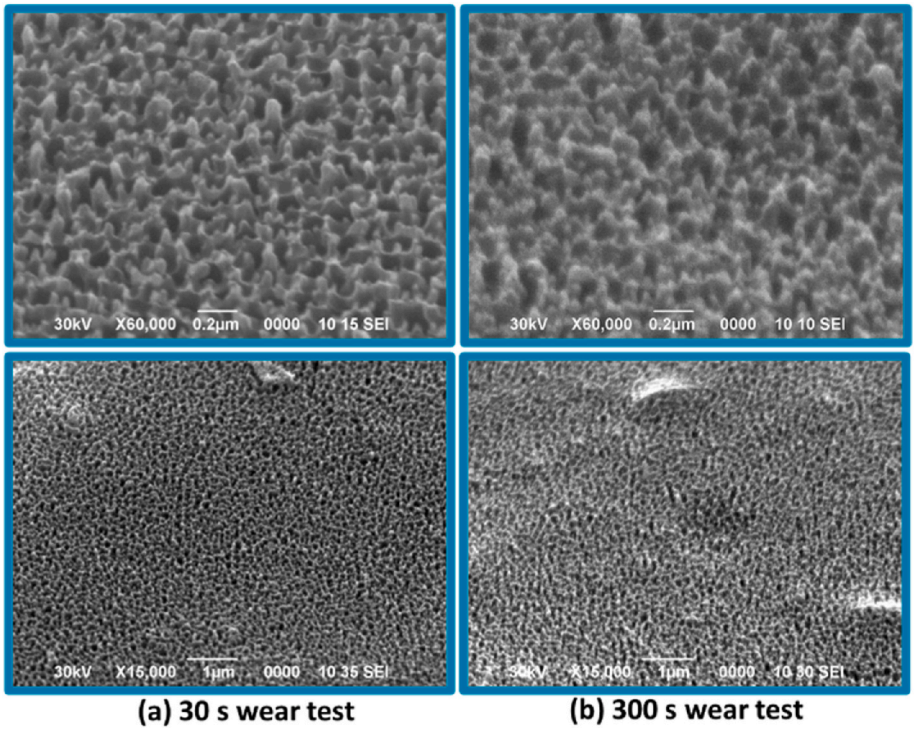

Fig. 5. SEM micrographs at 45° view angle for 2A100 after wear tests (30 s and 300 s), at 60000x (top) and 15000x magnification (bottom).

diameter as a result of a decrease in anodic oxide formation (Zaraska et al., 2016), which causes reduced growth of the oxide due to a lower current density when compared with oxalic acid. The higher voltage in the case of 2A100-2A (100 V) as compared to 2A50-2A (50 V) enhanced the chemical dissolution along the walls of the hexagon array, resulting in wider pores (62 nm vs 45 nm respectively) that are opened in the final etch. In the case of 1A50-2A vs 1A70-2A, while the pores in both cases have decreased size, the absolute difference in pore size is still similar. The second anodization had limited effect on pore size compared to the first anodization (compare 1A70-2A vs 2A100-2A for instance, where the latter was anodized a second time at 100 V while the former at 50 V). An increased wall thickness is observed in all cases after second anodization. Considering the structures after final etch, taller pillars are formed when 7 °C is used instead of 0 °C for the second anodization (while holding the same 50 V) —compare for instance 1A50 vs. 2A50, which might be related to the thickness of the oxide (and barrier) layer.

4.2. Nanopattern dimensions statistical analysis

For a robust comparison between the generated surfaces, a parametric (one-way ANOVA with Tukey HSD as post hoc test) and non-parametric test (Kruskal-Wallis with Wilcoxon as post hoc test) was made with a significance level of 0.05 (Fig. S2). Results show that all heights are statistically different. Pitch and FWHM differentiate even more 2A50 and 2A100 between them and 1A surfaces. Finally, tip widths are found to be different only when compared with 2A50. 1A50 and 1A70 have cone-like nanostructures with tall pillars (especially 1A70, with (384 ± 25) nm on average) while 2A50 and 2A100 have shorter heights (161 ± 15) and (200 ± 14) nm respectively); 2A50 also has significantly narrower pillars. These two geometries may have the lowest aspect ratio among all four, but they also resulted in the fewest defects, as 1A50 and 1A70 more commonly showed areas of collapsed pillars not accounted for in the statistical analysis.

4.3. Antimicrobial potential

Michalska et al. recently discussed the conditions that influence antibacterial activity in nanostructured substrates (Michalska et al., 2021), which can be summarized as material dependence (geometry, chemistry, stiffness, wettability), biological factors of the bacteria (cell wall properties, morphology, motility, properties of the extracellular polymeric substance), and environmental factors (nutrient media, pH, temperature, humidity, ionic strength of medium, air flow, time). In our case we tested under fixed biological and environmental conditions, while the geometry of the structures was varied (keeping the composition fixed). As shown in Fig. 6, the dried inoculum of *E. coli* in contact with the different surfaces evidences the interaction of bacteria with the nanostructures, particularly with the taller nanopillars. However, no obvious indication of cell lysis was present. To quantitatively assess the short-term effect of these surfaces on *E. coli*, cell viability was assayed after 60 min contact with aqueous inoculum, as detailed in the experimental section. This is within the timeframe for initial bacterial attachment towards biofilm formation, and a reasonable contact time to expect a reduction of bacteria viability for real-life, practical conditions (Sauer et al., 2002). The surfaces showed an average antibacterial activity of 47% *vs.* smooth Al controls which can be attributed to the nanotopography on the surfaces. As an ANOVA test concluded, there is no clear tendency between the nanopillar features and antibacterial activity for the contact time tested. The smooth aluminum samples produced 80% bacteriostatic efficiency compared to an agar control. While the intrinsic surface chemistry of the aluminum oxide surface is the main contributor to the antimicrobial effect, the nanostructures improve the bacteriostatic activity. The fact that in short contact time, distinct structures do not result in different antibacterial activity is a noteworthy result, as it implies a high tolerance in nanoscale features such as size and pitch should this kind of technology be of industrial interest. Antimicrobial assays with longer contact times are ongoing and the results will be made available in a future publication.

The nanopillar heights shown here are in the same order of magnitude as other reports; some nanopillars in the literature are taller, such

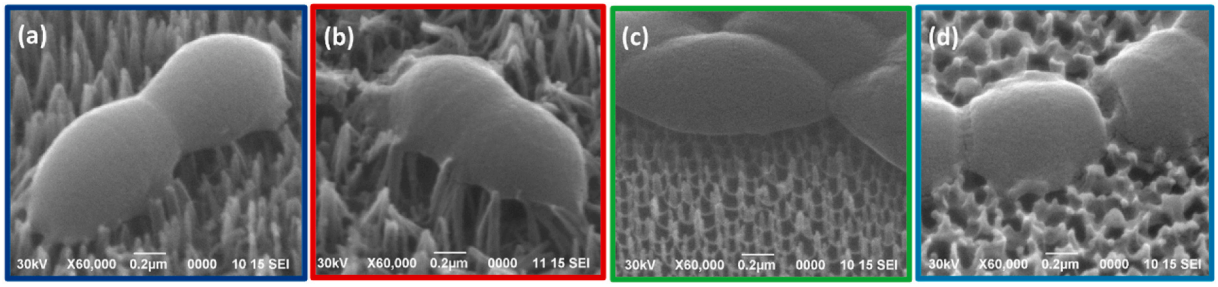

Fig. 6. Representative SEM images of *E. coli* on (a) 1A50 (b) 1A70 (c) 2A50 and (d) 2A100 samples (corresponding to those at the bottom of Fig. 2; low magnification images can be found in Fig. S5).

as black silicon (280/430/610 nm, with bactericidal activity of ~60% in 3 h for both *P. aeruginosa* and *S. aureus*) (Linklater et al., 2017) and boron-doped diamond coated black silicon pillars, ~1 μm tall) (May et al., 2016). Lower heights, such as the <100 nm tall titanium nanocolumns reported by Sengstock et al. resulted in ~60% bactericidal effect after 3 h with *E. coli* (no effect on *S. aureus*) according to fluorescence microscopy staining (Sengstock et al., 2014). In our case, the action of 1A50 against *E. coli* is not greater than 2A50 despite having taller pillars. Other factors such as the homogeneity of the nanopattern may have more influence. This follows the trend of other studies that show that small-tipped nanopillars in a close-packing arrangement maximize the mechanical stress experienced by bacteria (Velic et al., 2021). As Pirouz et al. recently reviewed (Pirouz et al., 2024), the processes through which the mechanical stress results in bacteria inactivation is still under study, since besides the possibility of cell wall rupture, cell wall localized deformation can lead to oxidative stress inside the cells, which can induce proteomic and genomic alterations with the bacteria (Le et al., 2023; Zhao et al., 2022).

Shorter structures are less prone to collapse and might lead to fewer defects, while taller nanostructures have more probability of having areas with collapsed pillars during the final etch or during sample manipulation, which can lead to lower antibacterial activity. As shown in Fig. 5, sample type 2A100 displays mechanical robustness to dry scrub with soft material (sponge) at typical human hand pressures, indicative of reusability after wiping; however, the other sample types showed nanopillar collapse even after only 30 s scrub cycles (Fig. S4), which would likely limit the structures to single use. The acceptable wear test behavior of 2A100 must be a consequence of the shorter and wider nanostructures that compose this sample type.

As shown in Fig. 7, fluorescence live/dead staining shows an abundance of live bacteria after 60 min of contact time; hence, the antimicrobial activity appears to be mostly bacteriostatic as opposed to bactericidal. However, mechano-bactericidal activity cannot be entirely dismissed at short contact times since other aluminum nanostructures have reported cell lysis (Hasan et al., 2020; Reed et al., 2019; Agbe et al., 2022b), and our SEM imaging shows bacteria membrane stretching.

As Pérez-Gavilán et al. discussed recently in their study with hydrophobic surfaces (Perez-Gavilan et al., 2021), misleading conclusions could be drawn when comparing substrate antibacterial activity measured using different protocols. The four nanopillared structures reported here show relevant antimicrobial potential in a short period of time using an adapted version of an international standard (Jeong and Choi, 2012), with the best surface having 57% of antibacterial activity in 60 min (2A100). In our approach we took bioinspiration from cicada and dragonfly wings which present nanopillars, and hence made the effort to generate this kind of structure for mechano-bacteriostatic effect in short term contact (1 h) with scalable wet chemistry. Our results are similar to those found with dragonfly wings in short contact spans, such as that of Bandara et al. (Bandara et al., 2017), who reported about 40% efficacy after 2 h contact time, and those of Ivanova et al. with their bioinspired black silicon, with *ca* 50% efficiency in 3 h contact time against *P. aeruginosa*, a prototypical gram-negative bacterium (Ivanova et al., 2013b).

5. Conclusions

We have developed a 4-step, potentially scalable process to generate different nanopillars from industrial aluminum alloy by modulating voltage and temperature conditions during anodization. Ranges of nanostructure dimensions are significant for height (161–384 nm), pitch (100–176 nm), and width at half maximum (50–122 nm). These structures might be useful for other applications in materials science, such as plasmonics, photonics, and catalysis, besides the bioinspired application showcased in this paper. While the intrinsic surface chemistry of the aluminum oxide surface is a significant contributor to the antimicrobial effect, the nanostructures improve the bacteriostatic activity. No statistical difference in antimicrobial activity is found despite the variation in dimensions. Fluorescence microscopy with live/dead kit after 1 h contact time showed few bacteria deaths. Hence, with our substrates, the likely scenario is that bacteria are mechanically stressed enough to preclude colony growth for approximately half of the bacteria vs electropolished aluminum. Further process engineering might lead to an optimized short term antimicrobial effect. It would be interesting to study the effect of longer contact times, and on gram-positive bacteria, such as *S. aureus*; these activities are planned and will be reported in a future publication. In addition, this passive strategy could be used in conjunction with active strategies, such as antibiotics for synergy effect (Díaz et al., 2012), and perhaps even regulate antibiotic resistance due

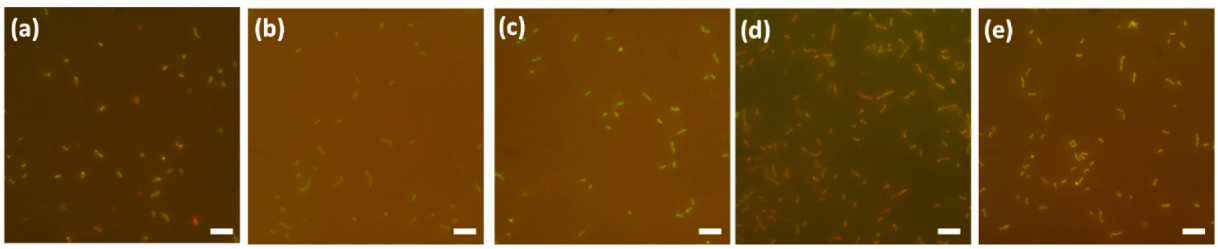

Fig. 7. Representative fluorescence microscopy images of live/dead kit-stained *E. coli* on nanotopographic substrates and smooth control after 60 min contact time. (a) 1A-50, (b) 1A-70, (c) 2A-50, (d) 2A-100, (e) electropolished aluminum control. Excitation at 450–490 nm with emission starting at 515 nm. Scale bar is 10 μm.

to physiological changes in bacteria (Genova et al., 2019). Except for 2A100, which passed an automated scrubbing test (5 min), the other substrates would likely be limited to single use if scrubbed at significant pressure (150 kPa) given their fine nanostructure.

CRediT authorship contribution statement

Gabriel Jiménez-Thuel: Writing – review & editing, Writing – original draft, Visualization, Methodology, Investigation, Formal analysis, Data curation. **Josué Cordero-Guerrero:** Writing – review & editing, Investigation. **Sergio Solano-Calderón:** Writing – review & editing, Investigation. **Sergio A. Paniagua:** Writing – review & editing, Writing – original draft, Visualization, Supervision, Resources, Project administration, Methodology, Investigation, Funding acquisition, Data curation, Conceptualization.

Ethical approval

Not applicable.

Declaration of competing interest

The authors declare the following financial interests/personal relationships which may be considered as potential competing interests: Sergio A. Paniagua reports financial support was provided by Office of Naval Research Global. If there are other authors, they declare that they have no known competing financial interests or personal relationships that could have appeared to influence the work reported in this paper.

Acknowledgments

This work was supported by Office of Naval Research Grant N62909-20-1-2031, and Centro Nacional de Alta Tecnología (CeNAT-CONARE) 2020–2021 and 2021–2022 scholarships. We thank CENIBIOT/CENAT for access to their fluorescence microscope. We acknowledge experimental support from Valery Conejo, Colombine Tavernier, Vanessa Jirón, Luis Carlos Murillo, Esteban Rojas, Nicolle Ujueta, Daniela Zúñiga, and Dr. Gabriela Montes de Oca. We are grateful to Jessica Nock Paniagua, Anthony J. Giordano, and Kassandra Cruz-Merazzo for proofreading, Dr. Joseph G. Manion for the assets and tutorials used for the scientific illustrations in this article, and Prof. José Vega Baudrit (LANOTEC Director) for his support.

Appendix A. Supplementary data

Supplementary data to this article can be found online at https://doi.org/10.1016/j.rsurfi.2025.100423.

Data availability statement

The data supporting this article have been included as part of the Supplementary Information.

References

Agbe, H., Sarkar, D.K., Chen, X.G., 2022a. Anodized aluminum surface with topography-mediated antibacterial properties. ACS Biomater. Sci. Eng. 8 (3), 1087–1095. https://doi.org/10.1021/acsbiomaterials.1c01485.

Agbe, H., Sarkar, D.K., Chen, X.G., 2022b. Anodized aluminum surface with topography-mediated antibacterial properties. ACS Biomater. Sci. Eng. 8 (3), 1087–1095. https://doi.org/10.1021/acsbiomaterials.1c01485.

Amir, A., Babaeipour, F., McIntosh, D.B., Nelson, D.R., Jun, S., 2014. Bending forces plastically deform growing bacterial cell walls. Proc. Natl. Acad. Sci. U.S.A. 111 (16), 5778–5783. https://doi.org/10.1073/pnas.1317497111.

Bandara, C.D., Singh, S., Afara, I.O., Wolff, A., Tesfamichael, T., Ostrikov, K., Oloyede, A., 2017. Bactericidal effects of natural nanotopography of dragonfly wing on Escherichia coli. ACS Appl. Mater. Interfaces 9 (8), 6746–6760. https://doi.org/10.1021/acsami.6b13666.

Cordero-Guerrero, J., Jiménez-Thuel, G., Paniagua, S.A., 2023. Sub-micron patterning of metal oxide surfaces via microcontact printing and microtransfer molding of amphiphilic molecules and antifouling application. J. Mater. Res. https://doi.org/10.1557/s43578-023-00909-x.

Cui, Q., Liu, T., Li, X., Song, K., Ge, D., 2020. Nanopillared polycarbonate surfaces having variable feature parameters as bactericidal coatings. ACS Appl. Nano Mater. 3 (5), 4599–4609. https://doi.org/10.1021/acsanm.0c00645.

Cui, Q., Liu, T., Li, X., Zhao, L., Wu, Q., Wang, X., et al., 2021. Validation of the mechano-bactericidal mechanism of nanostructured surfaces with finite element simulation. Colloids Surf. B Biointerfaces 206. https://doi.org/10.1016/j.colsurfb.2021.111929.

Díaz, C., Miñán, A., Schilardi, P.L., Fernández Lorenzo De Mele, M., 2012. Synergistic antimicrobial effect against early biofilm formation: micropatterned surface plus antibiotic treatment. Int. J. Antimicrob. Agents 40 (3), 221–226. https://doi.org/10.1016/j.ijantimicag.2012.05.012.

Elbourne, A., Crawford, R.J., Ivanova, E.P., 2017. Nano-structured antimicrobial surfaces: from nature to synthetic analogues. J. Colloid Interface Sci. https://doi.org/10.1016/j.jcis.2017.07.021. Academic Press Inc.

Fisher, L.E., Yang, Y., Yuen, M.-F., Zhang, W., Nobbs, A.H., Su, B., 2016. Bactericidal activity of biomimetic diamond nanocone surfaces. Biointerphases 11 (1), 011014. https://doi.org/10.1116/1.4944062.

Genova, L.A., Roberts, M.F., Wong, Y.-C., Harper, C.E., Santiago, A.G., Fu, B., et al., 2019. Mechanical stress compromises multicomponent efflux complexes in bacteria. https://doi.org/10.1073/pnas.1909562116/-/DCSupplemental.

Green, D.W., Lee, K.K.H., Watson, J.A., Kim, H.Y., Yoon, K.S., Kim, E.J., et al., 2017. High quality bioreplication of intricate nanostructures from a fragile gecko skin surface with bactericidal properties. Sci. Rep. 7. https://doi.org/10.1038/srep41023.

Hale, N., Valero, M., Tang, J., Moser, D., Jiang, L., 2018. A preliminary study on characterisation of finger interface kinetics using a pressure and shear sensor system. Prosthet. Orthot. Int. 42 (1). Retrieved from. https://journals.lww.com/poijournal/fulltext/2018/42010/a_preliminary_study_on_characterisation_of_finger.10.aspx.

Hall, C., 1997. External pressure at the hand during object handling and work with tools. Int. J. Ind. Ergon. 20 (3), 191–206. https://doi.org/10.1016/S0169-8141(96)00056-X.

Hasan, J., Xu, Y., Yarlagadda, T., Schuetz, M., Spann, K., Yarlagadda, P.K.D.V., 2020. Antiviral and antibacterial nanostructured surfaces with excellent mechanical properties for hospital applications. ACS Biomater. Sci. Eng. 6 (6), 3608–3618. https://doi.org/10.1021/acsbiomaterials.0c00348.

Hillebrand, R., Müller, F., Schwirn, K., Lee, W., Steinhart, M., 2008. Quantitative analysis of the grain morphology in self-assembled hexagonal lattices. ACS Nano 2 (5), 913–920. https://doi.org/10.1021/nn700318v.

Hizal, F., Rungraeng, N., Lee, J., Jun, S., Busscher, H.J., van der Mei, H.C., Choi, C.H., 2017. Nanoengineered superhydrophobic surfaces of aluminum with extremely low bacterial adhesivity. ACS Appl. Mater. Interfaces 9 (13), 12118–12129. https://doi.org/10.1021/acsami.7b01322.

Ivanova, E.P., Hasan, J., Webb, H.K., Truong, V.K., Watson, G.S., Watson, J.A., et al., 2012. Natural bactericidal surfaces: mechanical rupture of pseudomonas aeruginosa cells by cicada wings. Small 8 (16), 2489–2494. https://doi.org/10.1002/smll.201200528.

Ivanova, E.P., Hasan, J., Webb, H.K., Gervinskas, G., Juodkazis, S., Truong, V.K., et al., 2013a. Bactericidal activity of black silicon. Nat. Commun. 4. https://doi.org/10.1038/ncomms3838.

Ivanova, E.P., Hasan, J., Webb, H.K., Gervinskas, G., Juodkazis, S., Truong, V.K., et al., 2013b. Bactericidal activity of black silicon. Nat. Commun. 4, 1–7. https://doi.org/10.1038/ncomms3838.

Japanese Standards Association, 2000. Antimicrobial Products Test for Antimicrobial Activity and Efficacy, Japanese Industrial Standard JIS Z 2801. *Reference number: JIS Z 2801: 2000 (E), First English edition published in 2001*.

Jeong, C., Choi, C.H., 2012. Single-step direct fabrication of pillar-on-pore hybrid nanostructures in anodizing aluminum for superior superhydrophobic efficiency. ACS Appl. Mater. Interfaces 4 (2), 842–848. https://doi.org/10.1021/am201514n.

Kelleher, S.M., Habimana, O., Lawler, J., O'reilly, B., Daniels, S., Casey, E., Cowley, A., 2016. Cicada wing surface topography: an investigation into the bactericidal properties of nanostructural features. ACS Appl. Mater. Interfaces 8 (24), 14966–14974. https://doi.org/10.1021/acsami.5b08309.

Kotha, R., Strickland, D., Ayon, A.A., 2015. Nanowire fabrication in porous alumina tempalets produced by employing sulphuric, oxalic and phosphoric acids. Open J. Inorg. Non-Metallic Mater. 5 (3), 41–49. https://doi.org/10.4236/ojinm.2015.53005.

Kwon, J.T., Shin, H.G., Seo, Y.H., Kim, B.H., Lee, H.G., Lee, J.S., 2009. Simple fabrication method of hierarchical nano-pillars using aluminum anodizing processes. Curr. Appl. Phys. 9 (2 Suppl. L). https://doi.org/10.1016/j.cap.2008.12.034.

Le, P.H., Linklater, D.P., Aburto-Medina, A., Nie, S., Williamson, N.A., Crawford, R.J., et al., 2023. Apoptosis of multi-drug resistant Candida species on microstructured titanium surfaces. Adv. Mater. Interfac. 10 (34), 2300314. https://doi.org/10.1002/admi.202300314.

Lin, N., Berton, P., Moraes, C., Rogers, R.D., Tufenkji, N., 2018. Nanodarts, nanoblades, and nanospikes: mechano-bactericidal nanostructures and where to find them. Adv. Colloid Interface Sci. https://doi.org/10.1016/j.cis.2017.12.007. Elsevier B.V.

Linklater, D.P., Nguyen, H.K.D., Bhadra, C.M., Juodkazis, S., Ivanova, E.P., 2017. Influence of nanoscale topology on bactericidal efficiency of black silicon surfaces. Nanotechnology 28 (24), 245301. https://doi.org/10.1088/1361-6528/aa700e.

Linklater, D.P., de Volder, M., Baulin, V.A., Werner, M., Jessl, S., Golozar, M., et al., 2018. High aspect ratio nanostructures kill bacteria via storage and release of mechanical energy. ACS Nano 12 (7), 6657–6667. https://doi.org/10.1021/acsnano.8b01665.

Linklater, D.P., Baulin, V.A., Juodkazis, S., Crawford, R.J., Stoodley, P., Ivanova, E.P., 2021. Mechano-bactericidal actions of nanostructured surfaces. Nat. Rev. Microbiol. https://doi.org/10.1038/s41579-020-0414-z. Nature Research.

Lutey, A.H.A., Gemini, L., Romoli, L., Lazzini, G., Fuso, F., Faucon, M., Kling, R., 2018. Towards laser-textured antibacterial surfaces. Sci. Rep. 8 (1). https://doi.org/10.1038/s41598-018-28454-2.

Masuda, H., Satoh, M., 1996. Fabrication of gold nanodot array using anodic porous alumina as an evaporation mask. Jpn. J. Appl. Phys. (35). https://doi.org/10.1143/JJAP.35.L126.

May, P.W., Clegg, M., Silva, T.A., Zanin, H., Fatibello-Filho, O., Celorrio, V., et al., 2016. Diamond-coated 'black silicon' as a promising material for high-surface-area electrochemical electrodes and antibacterial surfaces. J. Mater. Chem. B 4 (34), 5737–5746. https://doi.org/10.1039/C6TB01774F.

Michalska, M., Gambacorta, F., Divan, R., Aranson, I.S., Sokolov, A., Noirot, P., Laible, P. D., 2018. Tuning antimicrobial properties of biomimetic nanopatterned surfaces. Nanoscale 10 (14), 6639–6650. https://doi.org/10.1039/C8NR00439K.

Michalska, M., Divan, R., Noirot, P., Laible, P.D., 2021. Antimicrobial properties of nanostructured surfaces – demonstrating the need for a standard testing methodology. Nanoscale 13 (41), 17603–17614. https://doi.org/10.1039/D1NR02953C.

Murata, T., Yamaguchi, K., Yanagishita, T., 2024. Antimicrobial activity of anodic porous alumina with controlled surface structures. Langmuir. https://doi.org/10.1021/acs.langmuir.4c02202.

Perez-Gavilan, A., de Castro, J.V., Arana, A., Merino, S., Retolaza, A., Alves, S.A., et al., 2021. Antibacterial activity testing methods for hydrophobic patterned surfaces. Sci. Rep. 11 (1). https://doi.org/10.1038/s41598-021-85995-9.

Pirouz, A., Papakonstantinou, I., Michalska, M., 2024. Antimicrobial mechanisms of nanopatterned surfaces—a developing story. Front. Chem. 12. Retrieved from. https://www.frontiersin.org/journals/chemistry/articles/10.3389/fchem.2024.1354755.

Pogodin, S., Hasan, J., Baulin, V.A., Webb, H.K., Truong, V.K., Phong Nguyen, T.H., et al., 2013. Biophysical model of bacterial cell interactions with nanopatterned cicada wing surfaces. Biophys. J. 104 (4), 835–840. https://doi.org/10.1016/j.bpj.2012.12.046.

Rauf, A., Mehmood, M., Asim Rasheed, M., Aslam, M., 2009. The effects of electropolishing on the nanochannel ordering of the porous anodic alumina prepared in oxalic acid. J. Solid State Electrochem. 13 (2), 321–332. https://doi.org/10.1007/s10008-008-0550-2.

Reed, J.H., Gonsalves, A.E., Román, J.K., Oh, J., Cha, H., Dana, C.E., et al., 2019. Ultrascalable multifunctional nanoengineered copper and aluminum for antiadhesion and bactericidal applications. ACS Appl. Bio Mater. 2 (7), 2726–2737. https://doi.org/10.1021/acsabm.8b00765.

Sauer, K., Camper, A.K., Ehrlich, G.D., Costerton, J.W., Davies, D.G., 2002. *Pseudomonas aeruginosa* displays multiple phenotypes during development as a biofilm. J. Bacteriol. 184 (4), 1140–1154. https://doi.org/10.1128/jb.184.4.1140-1154.2002.

Sengstock, C., Lopian, M., Motemani, Y., Borgmann, A., Khare, C., Buenconsejo, P.J.S., et al., 2014. Structure-related antibacterial activity of a titanium nanostructured surface fabricated by glancing angle sputter deposition. Nanotechnology 25 (19), 195101. https://doi.org/10.1088/0957-4484/25/19/195101.

Sharklet Technologies. (n.d.). Sharklet. from. https://sharklet.com/. (Accessed 30 April 2022).

Skara, 2016. Innovation and Future Trends in Food Manufacturing and Supply Chain Technologies. Elsevier.

Su, Z., Hähner, G., Zhou, W., 2008. Investigation of the pore formation in anodic aluminium oxide. J. Mater. Chem. 18 (47), 5787–5795. https://doi.org/10.1039/b812432a.

Sulka, G., 2008. Highly ordered anodic porous alumina formation by self-organized anodizing. In: Nanostructured Materials in Electrochemistry. Wiley-VCH, Germany.

Teshima, H., Kojima, K., Ju, Y., 2014. Fabrication of anodic aluminum oxide template and copper nanowire surface fastener. Journal of Electronic Packaging, Transactions of the ASME 136 (4). https://doi.org/10.1115/1.4028316.

Tripathy, A., Sen, P., Su, B., Briscoe, W.H., 2017. Natural and bioinspired nanostructured bactericidal surfaces. Adv. Colloid Interface Sci. https://doi.org/10.1016/j.cis.2017.07.030. Elsevier B.V.

Vassallo, E., Pedroni, M., Silvetti, T., Morandi, S., Toffolatti, S., Angella, G., Brasca, M., 2017. Bactericidal performance of nanostructured surfaces by fluorocarbon plasma. Mater. Sci. Eng. C 80, 117–121. https://doi.org/10.1016/j.msec.2017.05.111.

Velic, A., Jaggessar, A., Tesfamichael, T., Li, Z., Yarlagadda, P.K.D.V., 2021. Effects of nanopillar size and spacing on mechanical perturbation and bactericidal killing efficiency. Nanomaterials 11 (10). https://doi.org/10.3390/nano11102472.

Wandiyanto, J.V., Tamanna, T., Linklater, D.P., Truong, V.K., Al Kobaisi, M., Baulin, V. A., et al., 2020. Tunable morphological changes of asymmetric titanium nanosheets with bactericidal properties. J. Colloid Interface Sci. 560, 572–580. https://doi.org/10.1016/j.jcis.2019.10.067.

Watson, G.S., Green, D.W., Watson, J.A., Zhou, Z., Li, X., Cheung, G.S.P., Gellender, M., 2019. A simple model for binding and rupture of bacterial cells on nanopillar surfaces. Adv. Mater. Interfac. 6 (10). https://doi.org/10.1002/admi.201801646.

Xue, F., Liu, J., Guo, L., Zhang, L., Li, Q., 2015. Theoretical study on the bactericidal nature of nanopatterned surfaces. J. Theor. Biol. 385, 1–7. https://doi.org/10.1016/j.jtbi.2015.08.011.

Yi, L., Zhiyuan, L., Xing, H., Yisen, L., Yi, C., 2012. Investigation of intrinsic mechanisms of aluminium anodization processes by analyzing the current density. RSC Adv. 2 (12), 5164–5171. https://doi.org/10.1039/c2ra01050j.

Zaraska, L., Jaskuła, M., Sulka, G.D., 2016. Porous anodic alumina layers with modulated pore diameters formed by sequential anodizing in different electrolytes. Mater. Lett. 171, 315–318. https://doi.org/10.1016/j.matlet.2016.02.113.

Zhao, L., Liu, T., Li, X., Cui, Q., Wu, Q., Wang, X., et al., 2021. Low-temperature hydrothermal synthesis of novel 3D hybrid nanostructures on titanium surface with mechano-bactericidal performance. ACS Biomater. Sci. Eng. 7 (6), 2268–2278. https://doi.org/10.1021/acsbiomaterials.0c01659.

Zhao, S., Li, Z., Linklater, D.P., Han, L., Jin, P., Wen, L., et al., 2022. Programmed death of injured Pseudomonas aeruginosa on mechano-bactericidal surfaces. Nano Lett. 22 (3), 1129–1137. https://doi.org/10.1021/acs.nanolett.1c04243.